Separation and Purification Technology 329 (2024) 125183

Contents lists available at ScienceDirect

Separation and Purification Technology

journal homepage: www.elsevier.com/locate/seppur

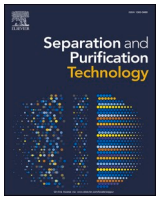

Efficient and selective Lead(II) removal within a wide concentration range through chemisorption and electrosorption coupling process *via* defective MoS_2 electrode

Weiquan Zhan [a,b,c], Yuan Yuan [a,b,d], Xuan Zhang [a,b], Yumeng Liang [a,b], Shaoxian Song [a,b,*], María de Jesús Martínez-López [e], José Luis Arauz-Lara [c], Feifei Jia [a,b,*]

[a] *Key Laboratory of Green Utilization of Critical Non-metallic Mineral Resources of Ministry of Education, Wuhan University of Technology, Wuhan, 430073, Hubei, China*
[b] *Hubei Key Laboratory of Mineral Resources Processing and Environment, Wuhan University of Technology, Wenzhi Street 34, Wuhan, Hubei, 430070, China*
[c] *Instituto de Fisica, Universidad Autonoma de San Luis Potosi, Zona Universitaria, Av. Manuel Nava 6, C.P. 78290, San Luis Potosi, Mexico*
[d] *Doctorado Institucional de Ingeniería y Ciencia de Materiales, Universidad Autonoma de San Luis Potosi, Av. Sierra Leona 530, San Luis Potosi, 78210, Mexico*
[e] *Universidad de la Costa, Carretera al Libramiento Paraje de Las Pulgas, Santiago Pinotepa Nacional, C.P. 71600, Distrito Jamiltepec, Mexico*

ARTICLE INFO

Keywords:
Lead(II) removal
Wide concentration range
Chemisorption and electrosorption coupling
Defective MoS_2 electrode

ABSTRACT

Developing method for efficient lead(II) removal from aqueous solutions over a wide concentration range is urgent but challenging. In this work, defective molybdenum disulfide (MoS_2) was served as electrode coating to capture lead(II) over a wide range from aqueous solution *via* chemisorption and electrosorption coupling (CEC) process. The distinct adsorption behaviors of lead(II) on defective MoS_2 electrode were theoretically and experimentally investigated. In a wide concentration range (1 ~ 100 mg/L), the removal efficiency of lead(II) from aqueous solutions can be close to ~ 100 %. Adsorption capacities for lead(II) removal at initial concentration of 8.37 and 18.71 mg/L were 64.99 and 159.98 mg/g, respectively. After applying voltage, adsorption capacity and removal efficiency were enhanced almost 8 folds due to strengthened migration of ions, electrostatic interaction and electric double layer. Besides, lead(II) was completely desorbed from defective MoS_2 electrode within 60 min, and defective MoS_2 electrode by CEC process maintained excellent regeneration ability even after 10 cycles. Defective MoS_2 electrode has shown superior properties for lead(II) removal, such as (i) great specific capacitance and (ii) low charge transfer resistance toward the enhanced adsorption capacity and diffusion for lead(II) in the electrical double layer, compared with MoS_2. Extensive computations and characterizations of defective MoS_2-lead(II) interaction demonstrated that the active unsaturated S sites were indispensable for lead(II) adsorption, which was beneficial for chemisorption. Based on the strong interaction with lead(II), defective MoS_2 electrode showed high-selectivity lead(II) adsorption with co-existence metal ions. Overall, defective MoS_2 as electrode coating by CEC has a great potential for the practical application in removing heavy metal ions from aquatic environment.

1. Introduction

Around the world, more challenges on water scarcity appears owing to increasing water demand and pollution, which is driven by the development of population and economics[1–3]. Considering the discharge of heavy metal ions from industry and mining, the increasing amount of heavy metal ions in aqueous solutions not only damages the environment but also threatens human health[4–6]. Among the existed heavy metal ions, lead(II) is taken as the common heavy metal ion with carcinogenicity[7]. Although various technologies and measures, including adsorption[8,9], chemical precipitation[10,11], electroadsorption[12], ion exchange[13,14], and membrane separation [15,16] have been developed to remove lead(II) from aqueous solutions, they only have advantages in removing lead(II) from low or high concentration, which results in the difficult industrial application. Therefore, it is vital to develop a mean to remove lead(II) over a wide concentration rage from aqueous solutions.

Electrosorption is a burgeoning approach with superiority of high

* Corresponding authors.
E-mail addresses: zhan_weiquan@163.com (W. Zhan), ssx851215@whut.edu.cn (S. Song), feifeijia@whut.edu.cn (F. Jia).

https://doi.org/10.1016/j.seppur.2023.125183
Received 15 August 2023; Received in revised form 18 September 2023; Accepted 22 September 2023
Available online 3 October 2023

energy efficiency and low environmental impact[17], while it is difficult to remove high concentrations of heavy metals. During the electrosorption process, two electrodes with a certain voltage are in parallel and solution flows inside the cell[18]. Generally, the charged ions move toward oppositely charged electrodes based on electric field and then be adsorbed, achieving the removal of objective ions[19]. If only voltage works in the process, the interaction between ions and electrodes is weak, thus it isn't efficient for removing high concentration of ions. Herein, removal of heavy metal ions with high concentration using electrosorption still remains a challenge.

Applying the materials on the surface of electrodes will enhance the physical and chemical interaction between ions and electrodes[20]. The ion removal ability depends on the electrical double layer, the affinity between material and ions at the interface. MoS_2 is a typically attractive material with abundant intrinsic sulfur atoms as well as low cost, non-toxicity, exhibiting great potential in heavy metal ions removal[21]. Based on the principle of hard and soft acids and bases (HSAB), sulfur atoms in MoS_2 are favorable for interaction with heavy metal ions[22]. Some studies[23–27] have reported the application of MoS_2 for heavy metal ions removal, such as mercury(II), lead(II), cadmium(II), cobalt (II) and chromium(IV). However, the affinity between heavy metal ions and MoS_2 still needs improvement for enhancing the driving force in application of high concentration removal.

The key to solve this problem is to find a way that allows enhanced chemisorption. It has been known that the adsorption of heavy metal ions in aqueous solution using MoS_2 due to its sulfur-rich characteristics and defects[28]. Besides, the chemical interaction between heavy metal ions and defects is stronger than that between heavy metal ions and intrinsic sulfur atoms. To the end, variety of defect-engineering strategies, plasma bombardment[29], chemical etching[30], template synthesis[31], solvothermal growth[32] and heteroatom doping[33] have been investigated. Among these methods, solvothermal growth attracts most attentions because of its easy operation and low cost [34].

Hence, defect-engineering was applied on MoS_2 in the work by adjusting the amount of thiourea with the purpose of enhancing chemisorption during the adsorption process. The defective MoS_2 as a coating was used in electrode for strengthening interaction between lead(II) and electrode, and not only electric filed force. During the process, combined chemisorption and electrosorption will benefit the heavy metal ions removal within a wide concentration range. Intrigued by the challenge, CEC could further extend the horizon of applications for removal or recovery of ions from aqueous solution. Defective MoS_2 is also expected to be bestowed with strong harvesting in the application of water treatment.

2. Methods

2.1. Reagents

Ammonium molybdate tetrahydrate ($(NH_4)_6Mo_7O_{24}{\cdot}4H_2O$), thiourea ($CN_2H_4S$), lead(II) nitrate ($Pb(NO_3)_2$), polytetrafluoroethylene ($(C_2F_4)n$), nitric acid (HNO_3), sodium hydroxide (NaOH), sodium chloride (NaCl), potassium chloride (KCl), calcium chloride ($CaCl_2$), magnesium chloride ($MgCl_2$), aluminum chloride hexahydrate ($AlCl_3{\cdot}6H_2O$), and iron chloride ($FeCl_3$) were all bought from Sinopharm Chemical Reagent Co., Ltd., China. Deionized water (a resistivity of 18.2 MΩ·cm) used in the experiment was produced though Millipore Super Q system.

2.2. Preparation

The synthesis of defective MoS_2 was through a simple hydrothermal way. Firstly, ammonium molybdate tetrahydrate ($(NH_4)_6Mo_7O_{24}{\cdot}4H_2O$) and thiourea ($CN_2H_4S$) were added into 32 mL deionized water for obtaining a homogeneous solution. Secondly, the solution was poured into a 50 mL Teflon-lined stainless-steel autoclave and heated at 220℃ for 18 h. Following, the container was cooled down to ambient temperature and then the products were washed with deionized water and ethanol. Finally, products were dried under −60℃ in vacuum for 12 h. Defective MoS_2 was prepared by adjusting the molar ratio of Mo and S source (1:2, 1:3, 1:4 and 1:5) *via* a hydrothermal route, and the corresponding obtained samples were named as MoS_2, D-MoS_2-1, D-MoS_2-2 and D-MoS_2-3.

2.3. Lead(II) removal experiments

The lead(II) removal electrode was fabricated through painting mixture including prepared samples (80 mg), conductive carbon black and polytetrafluoroethylene (mass ratio was 8:1:1) on rectangle titanium plate. Removal experiments were carried out in the device with an external power supply as shown in Fig. S1. 200 mL lead(II) solution with a certain concentration and pH was circulated at the rate of 45 rpm in the cell based on a peristatic pump (YZ1515x). Removal results were evaluated by adsorption capacity (Q) and removal (R) as follows:

$$Q = \frac{C_0 V - C_t V_t}{m} \tag{1}$$

$$R = \frac{C_0 - C_t}{C_0} \times 100\% \tag{2}$$

Where C_0 and C_t were the lead(II) concentration at the initial and t moment during the lead(II) removal experiment, respectively, mg/L; V and V_t represented volume of the solution at beginning and t moment, respectively, L; m meant the mass of samples used in the electrode, mg.

2.4. Reusability

The desorption of lead(II) in defective MoS_2 electrode was carried out by weakening the interaction between lead(II) and defective MoS_2. During the process, defective MoS_2 electrode was set as anode in the 0.2 M Na_2EDTA solution with 200 mL volume. The desorption efficiency was calculated as follows:

$$D_e = \frac{C_d V_d}{C_0 V} \times 100\% \tag{3}$$

Where C_d was the lead(II) concentration in Na_2EDTA solution during the lead(II) desorption experiment, mg/L; V_d exhibited the volume of desorption solution, mL; V meant the initial volume of removal experiment.

2.5. Characterizations

Crystal structure information was obtained by X-ray diffraction (XRD, D8 Advance, Bruker AXS, Germany) using Cu-Kα radiation. Particle size distribution of samples were analyzed by a Malvern Mastersizer 2000 (Malvern, England). Microstructures and corresponding energy dispersive spectra (EDS) were collected on scanning electron microscope (SEM, Phenom ProX G6, Netherlands) and transmission electron microscope (TEM, JEM-F200, Japan). Inductively coupled plasma-optical emission spectrometry (ICP-OES, Prodigy 7, America) was used to detect the chemical component analysis. Raman spectra were performed on an INVIA Raman microscope with an Ar laser (Renishaw, England). Chemical element state was done by X-ray photoelectron spectroscopy (XPS, Thermo Scientific ESCALAB Xi+, America). Electrochemical experiments including cyclic voltammetry (CV) and electrochemical impedance spectroscopy (EIS) were detected by a three-electrode system (VersaSTAT-450, PAR, U.S.A), and more information could be seen in the Section S1 of Supporting Information.

2.6. Density functional theory calculation

The interaction between lead(II) and defective MoS_2 was calculated using first principles calculation, which was performed by DMol3 program. The parameters for calculations were shown in the Supporting Information as Section S2. With the aim of studying stable configurations for defects, lack of a single atom and two atoms (Mo or S atom) in MoS_2 were considered, and as exhibited in Fig. 1a-h. In the Fig. 1a-d, the models were MoS_2 with Mo defects, and the blank part in an orange circle meant Mo vacancy. As for the configurations in Fig. 1e-h, they were MoS_2 with S defects, and the color of S atom in the orange circle is lighter than that in other part due to the loss of one upper S atom. Before calculating the interaction between lead(II) and defective MoS_2, the stability of defective MoS_2 was evaluated *via* the formation energy, as shown bellowed:

$$E_f = E_{dective} - E_{pure} + n\mu_{Mo} + m\mu_S \quad (4)$$

In which E_f was the formation energy; $E_{dective}$ and E_{pure} displayed the total energy of defective MoS_2 and MoS_2, respectively; μ_{Mo} and μ_S represented the chemical potentials of Mo and S, respectively; n and m were the vacancy numbers of Mo and S atoms, respectively.

Based on the calculation, the results were showed in Table S1. The formation energy of defective MoS_2 with S or Mo atom vacancy is positive, indicating that the formation of defective MoS_2 needs energy. Further, the formation energy of defective MoS_2 with S vacancy is lower than that with Mo atom vacancy, which displayed that the S vacancy is easier to form. Through the formation energies, the stable configurations of defective MoS_2 with one and two vacancies (Mo or S atoms) were selected for the calculation between lead(II) and defective MoS_2, and the corresponding electron density maps were showed in Fig. 1i-m. From the results, it demonstrated that Mo atoms could bind well with S atoms in all the defective structure.

3. Results and discussion

3.1. Structure and morphology analysis

The structure of the materials was determined by XRD (Fig. 2a). Intensive diffraction peaks at 13.91°, 33.31°, 39.44° and 59.02° that can be attributed to (002), (100), (103) and (110) of 2H MoS_2 (JCPDS 37–1492), respectively[35]. MoS_2 exhibited best crystallinity among the samples, while the diffraction peak strength decreased as the import of defects, which indicated that excessive of S atoms will weaken the crystallinity. When defects were introduced into structure, the atom interferometer direction was weakened. There aren't any other peaks, expressing that the change of dosage about Mo and S sources doesn't affect the structure of MoS_2. Raman spectroscopy was used for qualitatively evaluating the crystallinity and the degree of defects in MoS_2[36], and the corresponding results are displayed in Fig. 2b. The peaks located at 378.05 and 403.76 cm^{-1} can be ascribed to the E^1_{2g} and A_{1g} vibration of MoS_2. The E^1_{2g} mode means vibration mode of binding layer between Mo and S atoms, while A_{1g} mode corresponds to the out-of-plane vibration of S atoms[37]. The peaks at E^1_{2g} vibration of defective MoS_2 shifted to lower wavenumbers compared with MoS_2, demonstrating the formation of defects[38]. Furthermore, the smaller peak intensity ratio of E^1_{2g} and A_{1g}, the higher edge exposure [39]. From the Fig. S2, it showed that the E^1_{2g}/A_{1g} value decreased and then balanced with increased dosage of S source, which suggested that more defects occurred. Due to the stability of crystal structure, the number of defects in MoS_2 are limited. The quantitative data from Raman analyses of MoS_2 and defective MoS_2 was further confirmed by ICP test (Fig. 2c). Molar ratio of S and Mo increased, suggesting S atoms were enriched for defective MoS_2. The above defects could generate more active unsaturated atoms, and strongly affecting the electronic structure, which in turn improve the activity of active sites and the final properties[40].

The particle size distribution and morphologies of samples were

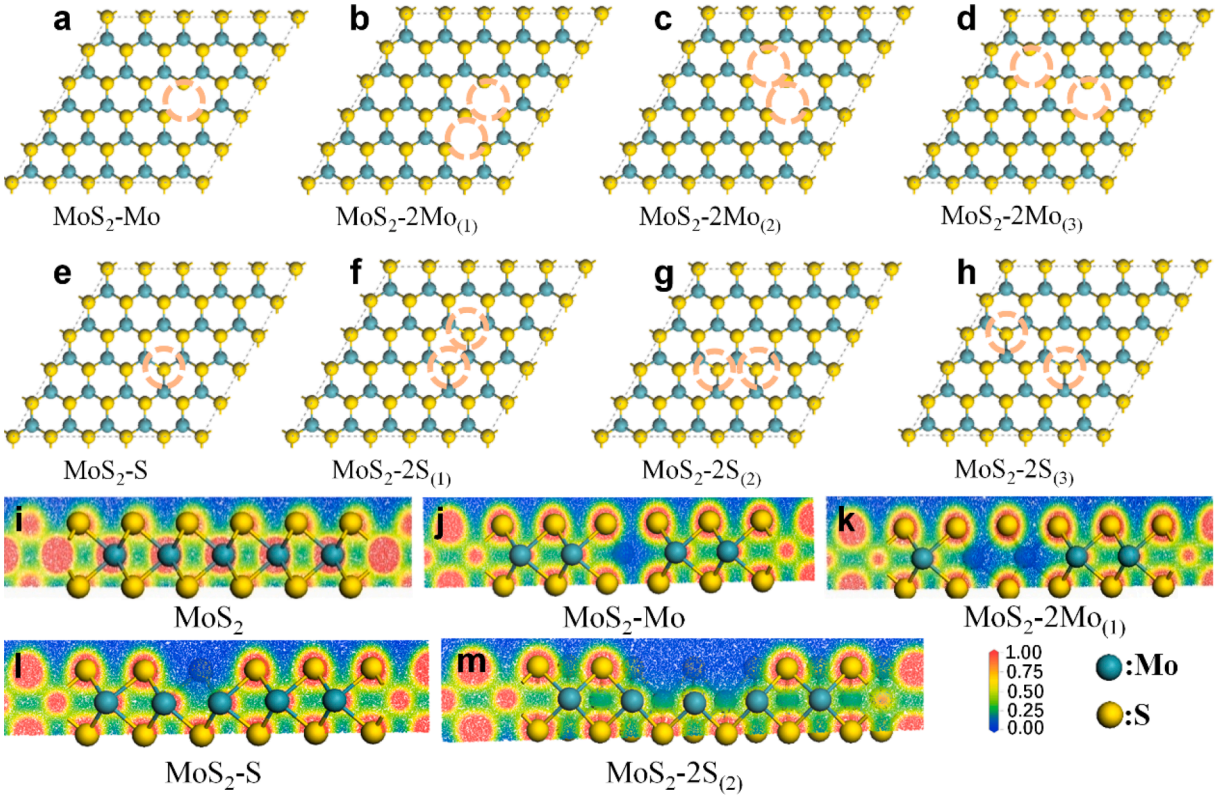

Fig. 1. The atomic configurations of defective MoS_2 with one or two vacancies: (a-d) Mo or (e-h) S atoms. Electron density maps of (i) MoS_2 and the stable configurations of defective MoS_2 with one atom or two vacancies: (j, k) Mo or (l, m) S atoms.

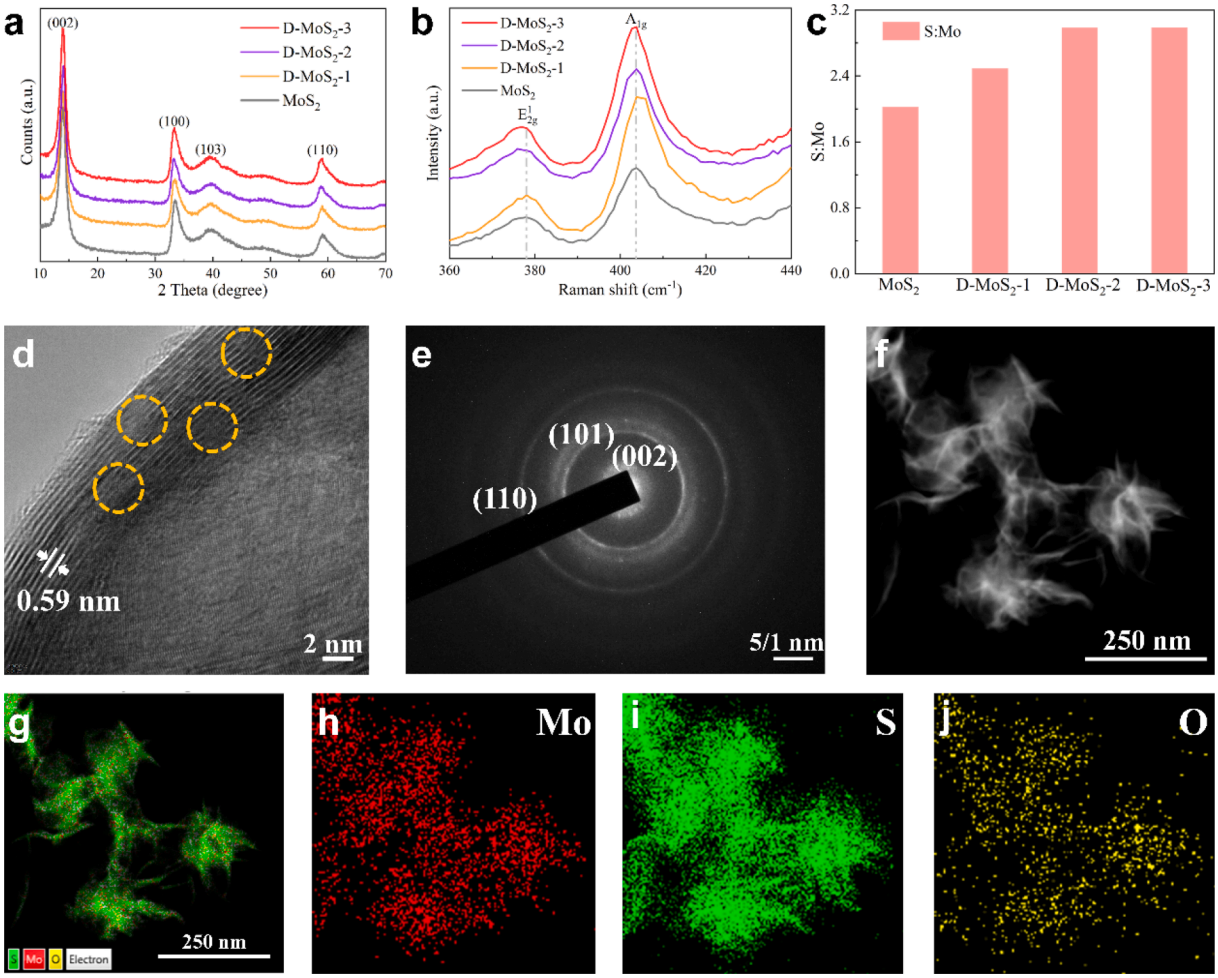

Fig. 2. (a) XRD patterns, (b) Raman spectra and (c) Molar ratio of S and Mo in ICP results of MoS_2 and defective MoS_2. (d) HRTEM image of defective MoS_2. Typical defects observed in orange circles and the interlayer distance of nanosheets. (e) Crystal facets of defective MoS_2. (f-g) TEM images and corresponding elemental mapping of defective MoS_2. (For interpretation of the references to color in this figure legend, the reader is referred to the web version of this article.)

characterized *via* Mastersizer, SEM and TEM. In Fig. S3, particle size at the D_{90} (particle size at 90 % cumulative undersize) became smaller as more sulfur source was introduced. It might be resulted from the hydrophobic agglomeration of MoS_2 with strong hydrophobic property. The results indicated that all the samples were in similar size distribution. From Fig. S4a-d, the SEM images of the synthesized samples displayed similar flower-like nanosheet morphology, which suggested that the dosage of S atoms didn't affect much on the morphology. TEM image (Fig. 2f) further confirmed that the nanosheets were uniformly distributed. Under the HRTEM observation, typical crystal lattices with spacing of 0.59 nm of defective MoS_2 is shown in Fig. 2d, which belonged to the (0 0 2) planes of MoS_2. The slightly alterative interlayer distance compared with the normal value (0.62–0.65 nm) maybe induced by the lattice distortion. The abundance of distorted areas in the synthesized defective MoS_2 marked by orange circles, is the evidence of disordered atomic arrangements or broken lamellar structures realized by excess of sulfur sources[41], which demonstrated the occurrence of defects. Other crystal facets belonging to (1 0 1) and (1 1 0) of MoS_2 appeared in SAED result (Fig. 2e). The homogeneous distribution of Mo and S throughout nanosheets the whole flower-like structure is demonstrated by the elemental mapping analysis in Fig. 2g-i and Fig. S4e-g. The existence of microscopic O element (Fig. 2j) was introduced through distortion of MoS_2, resulting from excess dosages of S atoms.

To further investigate the chemical component and prove the existence of defects in the structure of defective MoS_2, XPS measurements were carried out. The survey XPS in Fig. S5a confirmed the existence of Mo, S and O atoms. The peaks located at ~ 229.50, ~232.58 and ~ 226.70 eV are Mo $3d_{5/2}$, Mo $3d_{3/2}$ and S 2 *s* in the 2H phase MoS_2, respectively[42] (Fig. S5b). Furthermore, the deconvolution of Mo 3*d* peaks at 228.30 and 233.30 eV represented 1 T phase MoS_2, benefiting the transfer of electrons[43]. In Fig. S5c, two obvious peaks at ~ 162.50 and ~ 163.60 eV are attributed to the $2p_{3/2}$ and $2p_{1/2}$ peaks for the binding energy of S^{2-} chemical state in MoS_2[44]. Particularly, an additional peak was found in ~ 164.00 eV, which suggested the presence of defects in accordant with previous works[45]. The presence of O 1 *s* at ~ 532.21 eV was the evidence for –OH originated from the distortion[46] (Fig. S5d). The above consequences confirmed that the successful preparation of defective MoS_2.

3.2. Removal kinetics

The ability of defective MoS_2 electrode to removal lead(II) from aqueous solutions through CEC was explored as exhibited in Fig. 3. Apparently, compared the removal results between the electrode with and without samples as shown in Fig. 3a, b, no adsorption reaction appeared on titanium plate. Rapid removal of lead(II) happened by defective MoS_2 electrode under the low (8.37 mg/L) and high concentration (18.71 mg/L) in a short time. Subsequently, as time elapsed, the removal rate reached a plateau due to the saturated adsorption. The defective MoS_2 electrodes could reach close to 99.9 % removal efficiency of lead(II) in both low and high concentration at about 1240 min (Fig. 3b). For comprehensively expounding the adsorption process, two

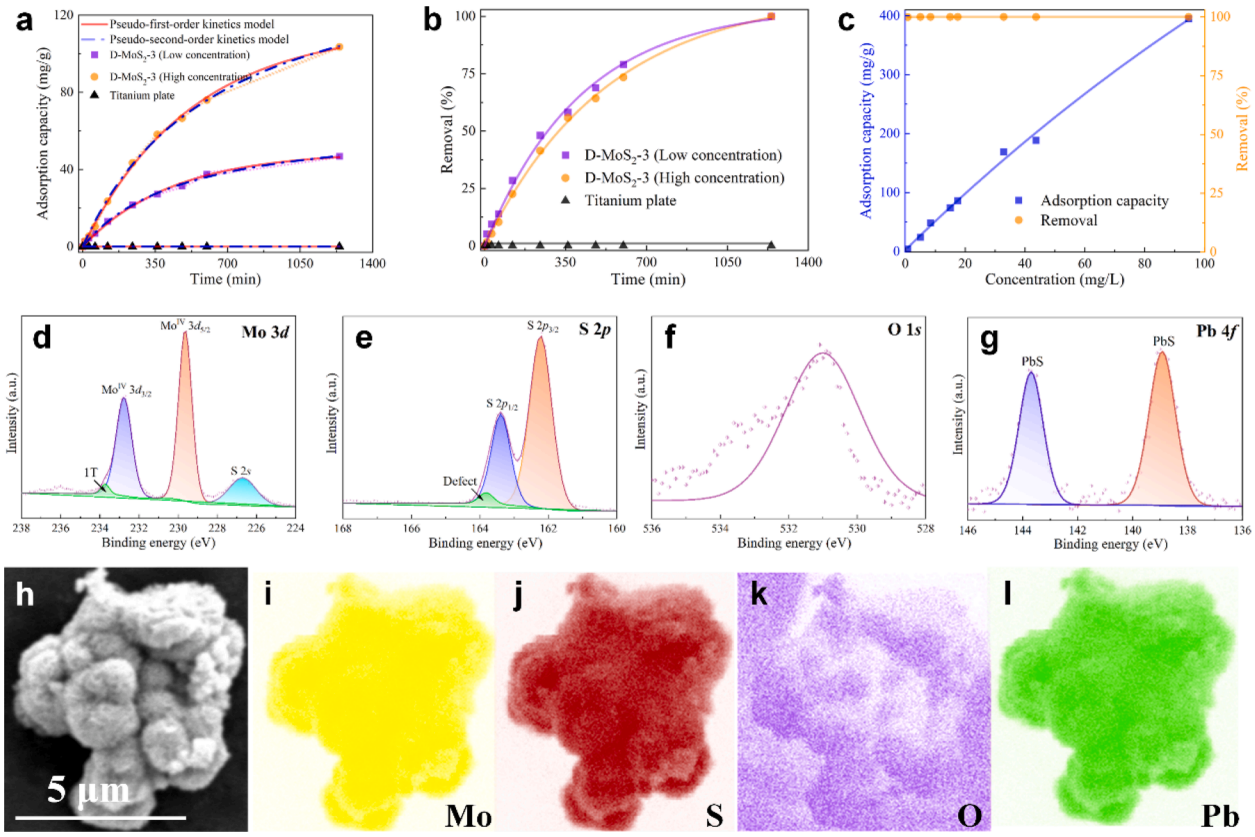

Fig. 3. Removal kinetics of lead(II) on defective MoS_2: (a) Adsorption capacity, (b) Removal. (c) Adsorption capacity and removal of lead(II) as a function of initial concentration. High-resolution XPS spectra of (d) Mo 3*d*, (e) S 2*p*, (f) O 1 *s* and (g) Pb 4*f* of defective MoS_2 after lead(II) removal. (h) SEM image and corresponding EDS element distribution mapping: (i) Mo, (j) S, (k) O and (l) Pb of defective MoS_2 after lead(II) removal.

typical kinetic models, the pseudo-first-order model and the pseudo-second-order model were utilized to fit the experimental data and the corresponding fitting parameters were summarized in Table 1. It can be evidently seen that the whole adsorption process was well depicted by the two models with advisable correlation coefficients, which exhibited that the lead(II) removal on defective MoS_2 was dominant by multiple interactions including physical and chemical adsorption. In low concentration, linear regression coefficients (R^2) in pseudo-first-order kinetic model (0.9963) was lower than that in pseudo-second-order kinetic model (0.9979), while on the contrary in high concentration. The results demonstrated that physical interaction was lightly stronger than chemical interaction in low concentration, but oppositely happened in high concentration. Furthermore, Elovich model (Fig. S6) and intraparticle diffusion model (Fig. S7) were used to fit the experimental data to study ion diffusion and adsorption mechanism, and related parameters were shown in Table 2. Elovich model was applied for researching the solutes removal from liquid solution. R^2 of 0.9479 and 0.9559 in low and high concentration displayed the unsuitability of this model. Diffusive mass transfer was expressed by interparticle diffusion model. Intraparticle curve didn't pass through the origin, and R^2 for all the concentration was poor, exhibiting that other mechanism like pseudo first or second order kinetic model except intraparticle diffusion play role in lead(II) removal[47,48]. Accordingly, the theoretical maximum adsorption capacities of lead(II) onto defective MoS_2 were calculated to be 64.99 and 159.98 mg/g in low and high concentration, respectively, which were evidently higher than that in previous works at the similar initial concentration as displayed in Table 3. During the removal process, the Mo concentration was detected for investigating the stability of defective MoS_2 electrode (Fig. S8). Little dissolution of Mo demonstrated that electrode had good stability for use. To explore the practical application of the method, defective MoS_2 electrode was used to test the adsorption capacity and removal efficiency of lead(II) in a wide concentration range, from 1 to 100 mg/L (Fig. 3c). The removal efficiency of lead(II) reached ~ 100 % within a wide concentration range. as the increase of initial concentration, the adsorption capacity increased, exhibiting that the defective MoS_2 electrode possessed rich adsorption

Table 2
Parameters of Elovich model and intraparticle diffusion model.

	Elovich			Intraparticle diffusion	
Concentration (mg/L)	β (mg/g)	α ((mg·g^{-1}·min^{-1})	R^2	K_i (mg·g^{-1}·min$^{-1/2}$)	R^2
8.37	9.5007	0.006095	0.9479	1.4874	0.9946
18.71	21.5096	0.002158	0.9559	3.4099	0.9906

Table 1
Kinetic parameters for lead(II) removal of psuodo-first-order model and pseudo-second-order morel.

	Pseudo-first-order kinetic model			Pseudo-second-order kinetic model		
Concentration (mg/L)	q_e (mg/g)	k_1 (min^{-1})	R^2	q_e (mg/g)	K_2 (min^{-1})	R^2
8.37	48.09	0.002	0.9963	64.99	0.000032	0.9979
18.71	113.93	0.00188	0.9990	159.98	0.000009	0.9987

Table 3
Comparison of the adsorption capacity in the work with others reported in literatures.

Adsorbents	Initial concentration (mg/L)	Adsorption capacity (mg/g)	Dosage (mg)	Temperature (℃)	References
CuS- Activated Carbon	9	33.00	9	Room	[51]
SnS-Activated Carbon	15	48.50	20	Room	[48]
Activated carbon	100	21.80	325	Room	[52]
Iron oxide	95	10.00	100	25	[53]
g-C_3N_4	10	65.60	2	25	[7]
HCl-treated Egyptian kaolin	100	34.50	100	25	[54]
KNTs	100	89.00	50	30	[55]
MoS_2 microflowers	100	99.10	50	25	[56]
CEC with	8.37	64.99	36	Room	This work
defective MoS_2	18.71	159.98			

sites for lead(II). This result indicated that the good performance was achieved by defective MoS_2 electrode in a wide concentration range.

To gain insight into the removal mechanism, XPS analysis was employed to identify and elucidate the intrinsic interaction between lead(II) and defective MoS_2. From the survey spectrum (Fig. S9), the characteristic peaks of lead(II) was found. Peaks in the spectra of Mo 3*d* and O 1 *s* (Fig. 3d and 3f) were similar with that in the structure of defective MoS_2 before lead(II) removal. For S 2*p* spectrum (Fig. 3e), after loading with lead(II), shifts of ~ 0.2 eV for peaks to a lower energy can be observed. These shifts indicated the formation of affinity between lead(II) and S atoms on defective MoS_2[49]. Fig. 3g shows the Pb 4*f* spectrum of defective MoS_2 after lead(II) removal, the lead(II) binding energies were centered at 138.9 and 143.7 eV for Pb $4f_{7/2}$ and Pb $4f_{5/2}$, respectively, confirming the strong interactions between S atoms and lead(II)[50]. According to the SEM image (Fig. 3h), defective MoS_2 after lead(II) removal maintained original characteristic morphology. The related EDS element distribution mapping (Fig. 3i-l) showed that the evenly distribution of Mo, S, O and Pb, indicating that the adsorption of lead(II) on the surface of defective MoS_2.

3.3. Removal performance of electrodes and environmental conditions

In order to investigate the effect of defective degree on removal performance, MoS_2 and defective MoS_2 were used as electrode to study adsorption capacity and removal of lead(II) in aqueous solutions at 1240 min (Fig. 4a). The adsorption capacity and removal by MoS_2 electrode were only ~ 19 mg/g and ~ 20 %, respectively. After the introduction of defects, the adsorption capacity and removal were obviously enhanced. As more sulfur atom resources added in the synthesized materials, the adsorption capacity and removal enhanced and then tend to balance, which related with the defective concentration (demonstrated in Raman and ICP results). The phenomenon clarified that the defects markedly facilitated the lead(II) removal during CEC. For instance, the adsorption capacity and removal by D-MoS_2-2 electrode were ~ 98 mg/g and ~ 99 %, respectively, which was almost 5 times than that using MoS_2.

The lead(II) removal performances affected by the distance of electrodes, voltage, pH were considered. As displayed in Fig. 4b, the adsorption capacity and removal under various distance between anode and cathode were almost the same, expressing that the distance didn't affect much on the lead(II) removal. Generally, the lead(II) removal process in aqueous solutions was dominant by electrostatic and chemical interaction, and the electrostatic interaction was related with the applied voltage on electrodes[57]. Hence, the removal behaviors of lead (II) toward defective MoS_2 under the condition of different voltage were investigated. In Fig. 4c, the adsorption capacity and removal for lead(II) increased when the voltage was presented. Apparently, the removal effects increased and then tended to stabilize, which is due to the lead(II) removal on defective MoS_2 reached saturation. In the CEC process, the electrostatic interaction between lead(II) and electrodes was enhanced. The solution pH could have a substantial influence on the ability of defective MoS_2 on lead(II) removal. pH ranging from 1.0 to 6.0 was investigated on the influence of lead(II) removal, as displayed in Fig. 4d, because lead(II) will precipitate[58] when pH is above 6.0 (Fig. S5). With the increase of pH, the adsorption capacity and removal of lead(II) in the solution were significantly enhanced, which was due to the competition of large number of H^+. The defective MoS_2 by CEC showed excellent lead(II) removal in a wide pH range (2 ~ 4), the removal closed to 100 % and the adsorption capacity up to 150 mg/g. One reason for the enhanced removal performance could be the increase of electrostatic interaction between lead(II) and electrodes, as displayed in Fig. 4e. While pH of solution not only influenced the surface potential of electrodes, but also changed the species of lead(II). When pH value was more than 4, the adsorption capacity and removal decreased might due to the generation of PbO_2 (Fig. S10), which would affect the active sites. Cationic was the most competitive ion for lead(II) removal in actual wastewater ([59]). Thus, the lead(II) removal efficiency in a binary-component solution (Na^+, K^+, Ca^{2+}, Mg^{2+}, Cd^{2+}, Al^{3+} and Fe^{3+}) was tested (Fig. 4f). The lead(II) removal could reach higher than ~ 90 % in the 20 mg/L for each metal ions. In addition, competition removal experiment in a mixing system was performed in Fig. S11, and it showed that CEC process with defective MoS_2 electrode had a good adsorption selectivity. The high selectivity was resulted from the strong interaction between lead(II) and defective MoS_2 and the low hydration energy of lead(II)[60].

3.4. Reusability

The reusability of electrodes and desorption mechanism were studied. The desorption of lead(II) was realized through changing defective MoS_2 electrode as anode in 0.2 M Na_2EDTA solution. Through applying defective MoS_2 electrode after adsorption as anode, lead(II) would be repulsed according to the electrostatic interaction. Meanwhile, the Na_2EDTA solution weakened the interaction between lead(II) and defective MoS_2[50]. As time elapsed, the desorption efficiency increased sharply, and it realized almost 100 % within 60 min (Fig. 5a). Then, the consecutive adsorption and desorption cycles were performed to evaluate the reusability of defective MoS_2 electrode. As displayed in Fig. 5b, the regenerated defective MoS_2 electrode could be reused 10 times, and the removal kept almost higher than 95 %. The original crystal structure, flower-like morphology and elemental distribution still maintained almost same as before after the regeneration of defective MoS_2 electrode for many times, as determined by Raman detection (Fig. 5c) and SEM-EDS test (Fig. 5d), respectively. This indicated that desorption would not affect much on the structure and morphology of defective MoS_2 electrode. In conclusion, the CEC method with defective MoS_2 electrode could be applied in practical water treatment.

3.5. Mechanism of lead(II) capture

The excellent lead(II) capture performance of defective MoS_2 was attributed to its chemisorption and electrosorption processes. To

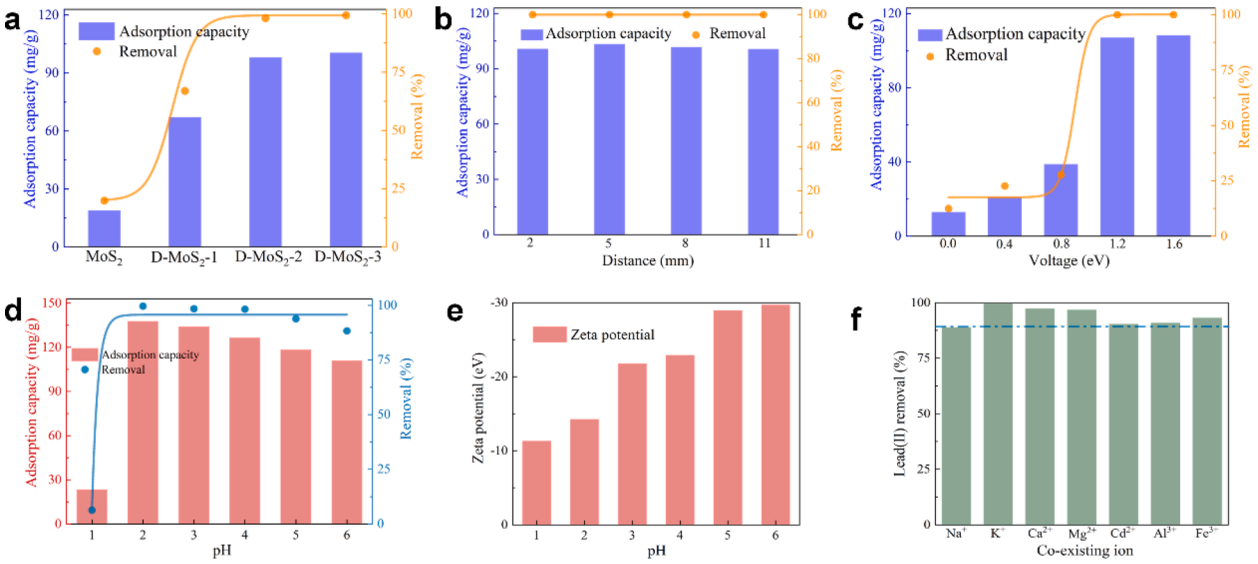

Fig. 4. Adsorption capacity and removal comparison of electrodes and environmental conditions with initial concentration of ~ 18 mg/g at 1240 min: (a) MoS_2 and defective MoS_2 electrode; (b) distance between electrodes; (c) voltage; (d) pH. (e) Zeta potential of defective MoS_2. (f) Effect of co-existing metal ions on lead(II) removal performance of defective MoS_2 electrode.

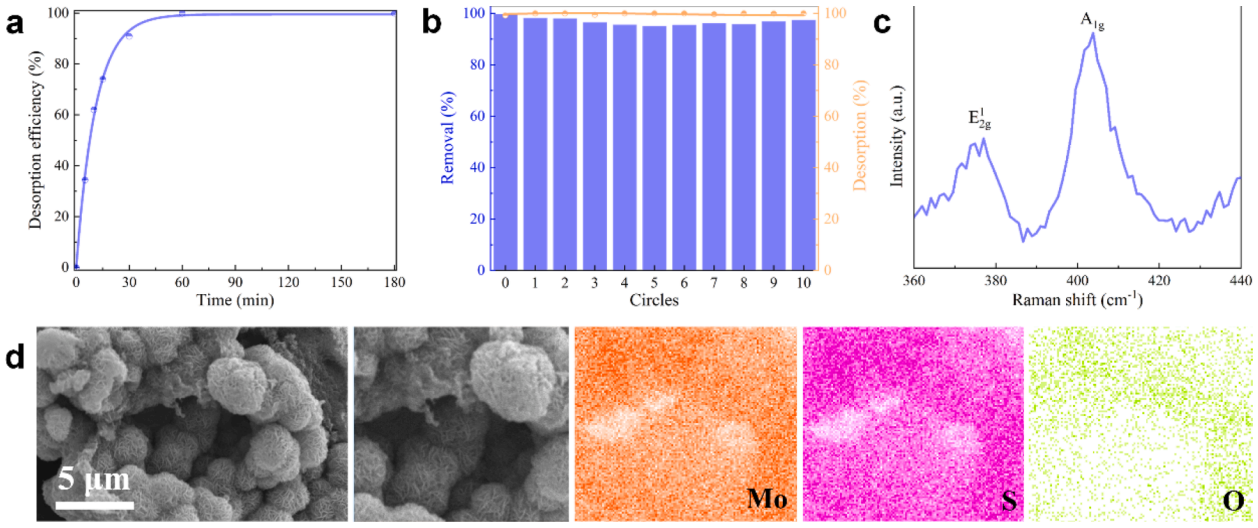

Fig. 5. (a) The desorption efficiency of lead(II) from defective MoS_2 electrode in Na_2EDTA solution. (b) Consecutive adsorption and desorption cycles of lead(II) using defective MoS_2 electrode. (c) Raman spectrum, (d) SEM image and corresponding EDS element distribution mapping: Mo, S, and O of defective MoS_2 electrode after regeneration.

precisely investigate the contributions of electric double layer, electrochemical performances of electrodes were conducted on the adsorption capacities[61]. The CV curves of MoS_2 and defective MoS_2 showed near-rectangular shapes (Fig. 6a), exhibiting the typical behaviors of electric double layer capacitance. Besides, as the introduction of defects, larger area of CV curve appeared, higher specific capacitance, which was beneficial for the adsorption of ions. CV curves of defective MoS_2 were recorded at various scan rates (Fig. 6b), and a good rectangular shape could be kept even at high scan rate, suggesting that lead(II) had enough time to diffuse and go through the structure of defective MoS_2. EIS was performed on the research of the intrinsic resistance of MoS_2 and defective MoS_2 (Fig. 6c). Compared defective MoS_2 with MoS_2, the semicircle in Nyquist plots was smaller, revealing a decrease of the charge transfer resistance when defects appeared. Moreover, the resistance was smallest in D-MoS_2-3, which was better for ions transport during the lead(II) removal process. Thus, after the generation of defects, increasing specific capacitance and lowing charge transfer resistance leaded to improve electrochemical performance, which improved electrosorption process of lead(II).

To better understand the phenomenon of interaction between lead (II) and defective MoS_2, the effects of Mo vacancy, S vacancy and defective degree on lead(II) removal performances were recorded based on DFT. From Fig. 6d-f, the charge overlap phenomenon could be obviously observed for both lead(II) and coordinated S atoms in the system of MoS_2 and defective MoS_2, which meant the formation of a chemical bond between lead(II) and S atoms[62]. The interaction between lead(II) and unsaturated S atoms was stronger than that in lead(II) with saturated S atoms. Compared with Fig. 6e and 6f, the S atoms with more unsaturated content in the presence of Mo vacancy bound tighter with lead(II) than that in the presence of S vacancy, which was also proved in the results of interaction energy (Fig. 6g). With more defective degrees, as displayed in Fig. 6g, the interaction energy between lead(II) and MoS_2 will be obviously enhanced. To further distinguish the phenomenon of bonding nature, partial density of state (PDOS) analysis was

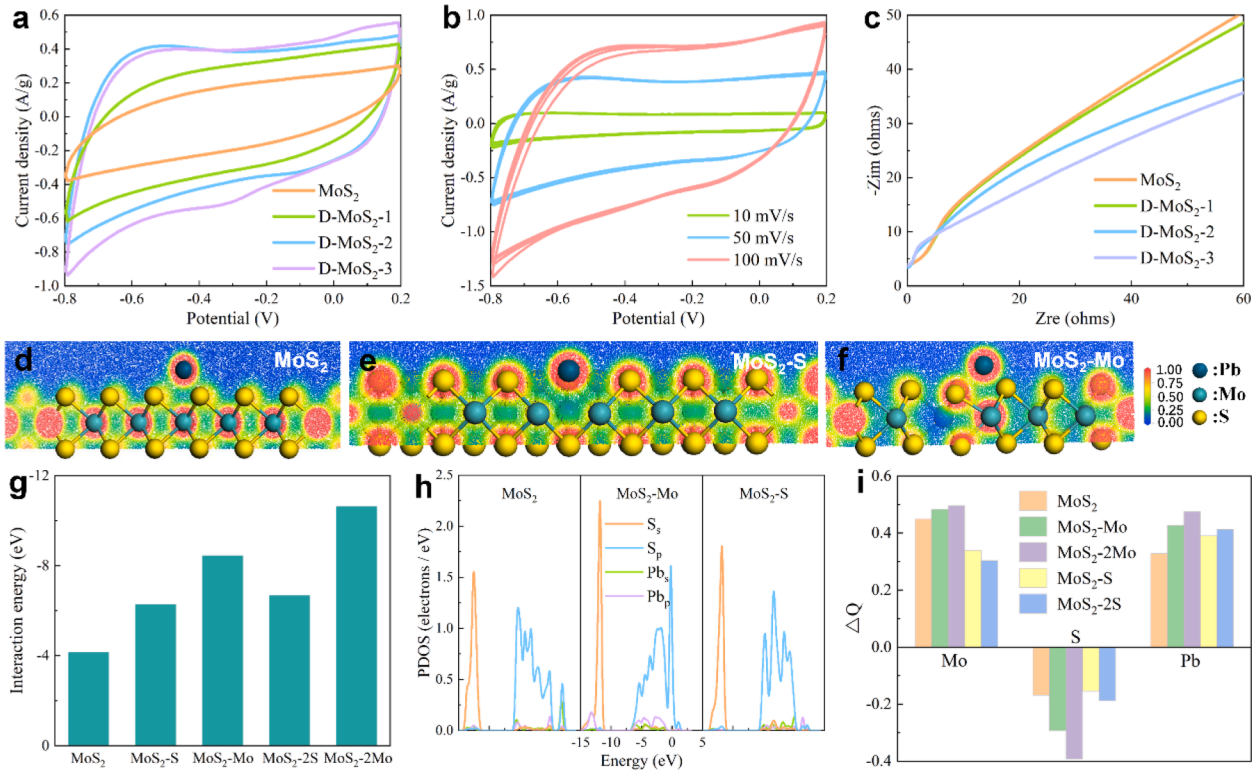

Fig. 6. (a-c) Side views of electron density maps and (d) interaction energy of lead(II) on MoS_2 and defective MoS_2. (e) PDOS of lead(II) and S atoms in the adsorption of lead(II) on MoS_2 and defective MoS_2. (f) Milliken atomic charges changes of lead(II), Mo atoms and S atoms nearby interacted parts in the systems of lead(II) adsorption on MoS_2 and defective MoS_2.

performed (Fig. 6h). It was clearly shown that the contribution of the DOS of lead(II) was mainly by $6p^2$ orbital. The bonding between Pb_p orbital and S_p in MoS_2 with Mo vacancy was stronger than that in the presence of S vacancy. When S atoms were more unsaturated, it showed higher reactivity in the bonding process with more empty orbitals. Milliken atomic charges analysis (Fig. 6i) further indicated that lead(II) contributed electrons to S atoms in MoS_2 and defective MoS_2, and more electrons were transferred in MoS_2 with Mo and S vacancy. In the presence of Mo vacancy, more electrons will be lost in S atoms to nearby Mo atoms and lead(II), which meant there is a competition between Mo atoms and lead(II) with S atoms. Additionally, Mo atoms contributed less electrons in MoS_2 with S vacancy compared that in MoS_2, demonstrating that lead(II) exhibited a stronger affinity with S atoms than Mo atoms with S atoms. S atoms in MoS_2 with S vacancy gained less charge electrons than that in MoS_2, which was due to the average distraction of charge electrons in lead(II) as showed in Fig. 6b. The lead(II) was in the center of unsaturated atoms, and the distance was farer away from than that in MoS_2 and MoS_2 with Mo vacancy.

4. Conclusions

In summary, an efficient lead(II) removal from aqueous solutions over a wide concentration range through CEC *via* defective MoS_2 electrode was originally demonstrated. The removal efficiency of lead(II) in low and high concentration (1 ~ 100 mg/L) was close to 100 %. Lead(II) could be totally removed from defective MoS_2 electrode in 60 min, and the defective MoS_2 electrode owned super removal ability even after 10 circles. Defective MoS_2 electrode has exhibited superior properties compared with MoS_2, such as (i) higher specific capacitance, (ii) lower charge transfer resistance and (iii) stronger interaction with lead(II), which enhanced the electrosorption and chemisorption. DFT calculations confirmed that unsaturated S atoms were the active adsorption site and responsible for the lead(II) binding. These evidences suggest that the electrochemical system equipped with the CEC could be an easy and efficient way for the removal of heavy metal ions in the future.

CRediT authorship contribution statement

Weiquan Zhan: Writing – original draft, Formal analysis, Methodology, Investigation. **Yuan Yuan:** Supervision, Methodology. **Xuan Zhang:** Formal analysis, Methodology. **Yumeng Liang:** Software, Investigation. **Shaoxian Song:** Writing – review & editing, Data curation. **María de Jesús Martínez-López:** Conceptualization. **José Luis Arauz-Lara:** Formal analysis. **Feifei Jia:** Data curation, Supervision.

Declaration of Competing Interest

The authors declare that they have no known competing financial interests or personal relationships that could have appeared to influence the work reported in this paper.

Data availability

Data will be made available on request.

Acknowledgements

The work is financially supported by the Natural Science Foundation of Hubei Province (ZRJQ2022000195). Zhan gratefully acknowledges the Consejo Nacional de Ciencia y Tecnología (CONACYT) of Mexico for offering him the scholarship under the grant No. 813934 during his Ph. D. studies.

Appendix A. Supplementary data

Supplementary data to this article can be found online at https://doi.

org/10.1016/j.seppur.2023.125183.

References

[1] M. Mao, T. Yan, J. Shen, J. Zhang, D. Zhang, Capacitive removal of heavy metal ions from wastewater via an electro-Adsorption and electro-reaction coupling process, Environ. Sci. Tech. 55 (2021) 3333–3340, https://doi.org/10.1021/ACS.EST.0C07849.

[2] Y. Peng, H. Huang, Y. Zhang, C. Kang, S. Chen, L. Song, D. Liu, C. Zhong, A versatile MOF-based trap for heavy metal ion capture and dispersion, Nat. Commun. 9 (2018) 1–9, https://doi.org/10.1038/s41467-017-02600-2.

[3] P. Goyal, D. Menon, P. Jain, P. Prakash, S.K. Misra, Linker mediated enhancement in reusability and regulation of Pb(II) removal mechanism of Cu-centered MOFs, Sep. Purif. Technol. 318 (2023), 123941, https://doi.org/10.1016/J.SEPPUR.2023.123941.

[4] C. Liu, T. Wu, P.C. Hsu, J. Xie, J. Zhao, K. Liu, J. Sun, J. Xu, J. Tang, Z. Ye, D. Lin, Y. Cui, Direct/alternating current electrochemical method for removing and recovering heavy metal from water using graphene oxide electrode, ACS Nano 13 (2019) 6431–6437, https://doi.org/10.1021/ACSNANO.8B09301.

[5] S. Bolisetty, R. Mezzenga, Amyloid–carbon hybrid membranes for universal water purification, Nat. Nanotechnol. 11 (2016) 365–371, https://doi.org/10.1038/nnano.2015.310.

[6] A. Lu, Z.Y. Zhang, D. Zhao, K. Zhu, Z. Li, Y. Wang, C. Hou, X.C. Shen, C. Ruan, High-efficiency and selective removal of Hg(II) and Pb(II) ions from aquatic system by 1T/2H mixed-phase $MoSe_2$ nanoflowers: Performance and mechanism, Sep. Purif. Technol. 318 (2023), 123982, https://doi.org/10.1016/J.SEPPUR.2023.123982.

[7] R. Hu, X. Wang, S. Dai, D. Shao, T. Hayat, A. Alsaedi, Application of graphitic carbon nitride for the removal of Pb(II) and aniline from aqueous solutions, Chem. Eng. J. 260 (2015) 469–477, https://doi.org/10.1016/J.CEJ.2014.09.013.

[8] L.L. Ling, W.J. Liu, S. Zhang, H. Jiang, Magnesium oxide embedded nitrogen self-doped biochar composites: Fast and high-efficiency adsorption of heavy metals in an aqueous solution, Environ. Sci. Tech. 51 (2017) 10081–10089, https://doi.org/10.1021/ACS.EST.7B0238.

[9] F. Zhang, X. Tang, Y. Huang, A.A. Keller, J. Lan, Competitive removal of Pb^{2+} and malachite green from water by magnetic phosphate nanocomposites, Water Res. 150 (2019) 442–451, https://doi.org/10.1016/J.WATRES.2018.11.057.

[10] Y. Wu, H. Pang, Y. Liu, X. Wang, S. Yu, D. Fu, J. Chen, X. Wang, Environmental remediation of heavy metal ions by novel-nanomaterials: A review, Environ. Pollut. 246 (2019) 608–620, https://doi.org/10.1016/J.ENVPOL.2018.12.076.

[11] S. Park, W.J. Chang, C.W. Lee, S. Park, H.Y. Ahn, K.T. Nam, Photocatalytic hydrogen generation from hydriodic acid using methylammonium lead iodide in dynamic equilibrium with aqueous solution, Nat. Energy 2 (2016) 1–8, https://doi.org/10.1038/nenergy.2016.185.

[12] J. Lu, P. Kumar Mishra, T.N. Hunter, F. Yang, Z. Lu, D. Harbottle, Z. Xu, Functionalization of mesoporous carbons derived from pomelo peel as capacitive electrodes for preferential removal/recovery of copper and lead from contaminated water, Chem. Eng. J. 433 (2022), 134508, https://doi.org/10.1016/J.CEJ.2022.134508.

[13] M.A. Alkhadra, M.L. Jordan, H. Tian, C.G. Arges, M.Z. Bazant, Selective and chemical-free removal of toxic heavy metal cations from water using shock ion extraction, Environ. Sci. Tech. 56 (2022) 14091–14098, https://doi.org/10.1021/ACS.EST.2C05042.

[14] Q. Peng, J. Guo, Q. Zhang, J. Xiang, B. Liu, A. Zhou, R. Liu, Y. Tian, Unique lead adsorption behavior of activated hydroxyl group in two-dimensional titanium carbide, J. Am. Chem. Soc. 136 (2014) 4113–4116, https://doi.org/10.1021/JA500506K.

[15] Z. Wang, Q. Tu, A. Sim, J. Yu, Y. Duan, S. Poon, B. Liu, Q. Han, J.J. Urban, D. Sedlak, B. Mi, Superselective removal of lead from water by two-dimensional MoS_2 nanosheets and layer-stacked membranes, Environ. Sci. Tech. 54 (2020) 12602–12611, https://doi.org/10.1021/ACS.EST.0C02651.

[16] L. Wang, L. Deligniere, S. Husmann, R. Leiner, C. Bahr, S. Zhang, C. Dun, M. M. Montemore, M. Gallei, J.J. Urban, C. Kim, V. Presser, Selective Pb^{2+} removal and electrochemical regeneration of fresh and recycled FeOOH, Nano Res. (2023) 1–12, https://doi.org/10.1007/S12274-023-5569-2/METRICS.

[17] G. Zhou, J. Luo, C. Liu, L. Chu, J. Crittenden, Efficient heavy metal removal from industrial melting effluent using fixed-bed process based on porous hydrogel adsorbents, Water Res. 131 (2018) 246–254, https://doi.org/10.1016/J.WATRES.2017.12.067.

[18] J.K. Alagarasan, S. Shasikala, E.R. Rene, P. Bhatt, P. Thangavelu, P. Madheswaran, S. Subramanian, D.D. Nguyen, S.W. Chang, M. Lee, Electro-oxidation of heavy metals contaminated water using banana waste-derived activated carbon and Fe_3O_4 nanocomposites, Environ. Res. 215 (2022), 114293, https://doi.org/10.1016/J.ENVRES.2022.114293.

[19] X. Chen, D. Chen, N. Li, Q. Xu, H. Li, J. He, J. Lu, Modified-MOF-808-loaded polyacrylonitrile membrane for highly efficient, simultaneous emulsion separation and heavy metal ion removal, ACS Appl. Mater. Interfaces 12 (2020) 39227–39235, https://doi.org/10.1021/ACSAMI.0C10290.

[20] Y. Sun, Y. Su, Z. Zhao, J. Zhao, M. Ye, X. Wen, Capacitive heavy metal ion removal of 3D self-supported nitrogen-doped carbon-encapsulated titanium nitride nanorods via the synergy of faradic-reaction and electro-adsorption, Chem. Eng. J. 443 (2022), 136542, https://doi.org/10.1016/J.CEJ.2022.136542.

[21] B. Radisavljevic, A. Radenovic, J. Brivio, V. Giacometti, A. Kis, Single-layer MoS_2 transistors, Nat. Nanotechnol. 6 (2011) 147–150, https://doi.org/10.1038/nnano.2010.279.

[22] W. Zhan, F. Jia, Y. Yuan, C. Liu, K. Sun, B. Yang, Controllable incorporation of oxygen in MoS_2 for efficient adsorption of Hg^{2+} in aqueous solutions, J. Hazard. Mater. 384 (2020) 1–10, https://doi.org/10.1016/j.jhazmat.2019.121382.

[23] W. Zhan, Y. Yuan, C. Liu, P. Chen, Y. Liang, Y. Wang, J.L. Arauz-Lara, F. Jia, Preparation and application of 0D, 2D and 3D molybdenite: a review, Minerals and Mineral Materials. 1 (2022) 5, https://doi.org/10.20517/mmm.2022.04.

[24] W. Yin, X. Dong, J. Yu, J. Pan, Z. Yao, Z. Gu, Y. Zhao, MoS_2-Nanosheet-assisted coordination of metal ions with porphyrin for rapid detection and removal of cadmium ions in aqueous media, ACS Appl. Mater. Interfaces 9 (2017) 21362–21370, https://doi.org/10.1021/ACSAMI.7B04185.

[25] C. Pan, L. Fu, Y. Ding, X. Peng, Q. Mao, Homogeneous catalytic activation of peroxymonosulfate and heterogeneous reductive regeneration of Co^{2+} by MoS_2: The pivotal role of pH, Sci. Total Environ. 712 (2020), 136447, https://doi.org/10.1016/J.SCITOTENV.2019.136447.

[26] K. Ai, C. Ruan, M. Shen, L. Lu, MoS_2 nanosheets with widened interlayer spacing for high-efficiency removal of mercury in aquatic systems, Adv. Funct. Mater. 26 (2016) 5542–5549, https://doi.org/10.1002/ADFM.201601338.

[27] T.H. Gu, J. Kim, S.M. Oh, X. Jin, S.J. Hwang, Interstratified heterostructures of metal hydroxide nanoclusters and MoS_2 monolayers with improved electrode performance, Nanoscale 12 (2020) 11759–11766, https://doi.org/10.1039/D0NR02569K.

[28] X. Wang, Y. Zhang, H. Si, Q. Zhang, J. Wu, L. Gao, X. Wei, Y. Sun, Q. Liao, Z. Zhang, K. Ammarah, L. Gu, Z. Kang, Y. Zhang, Single-atom vacancy defect to trigger high-efficiency hydrogen evolution of MoS_2, J. Am. Chem. Soc. 142 (2020) 4298–4308, https://doi.org/10.1021/JACS.9B12113.

[29] J. Zhu, Z. Wang, H. Yu, N. Li, J. Zhang, J. Meng, M. Liao, J. Zhao, X. Lu, L. Du, R. Yang, D. Shi, Y. Jiang, G. Zhang, Argon plasma induced phase transition in monolayer MoS_2, J. Am. Chem. Soc. 139 (2017) 10216–10219, https://doi.org/10.1021/JACS.7B05765.

[30] P. Zhang, H. Xiang, L. Tao, H. Dong, Y. Zhou, T.S. Hu, X. Chen, S. Liu, S. Wang, S. Garaj, Chemically activated MoS_2 for efficient hydrogen production, Nano Energy 57 (2019) 535–541, https://doi.org/10.1016/J.NANOEN.2018.12.045.

[31] L. Gao, Q. Liao, X. Zhang, X. Liu, L. Gu, B. Liu, J. Du, Y. Ou, J. Xiao, Z. Kang, Z. Zhang, Y. Zhang, Defect-engineered atomically thin MoS_2 homogeneous electronics for logic inverters, Adv. Mater. 32 (2020) 1906646, https://doi.org/10.1002/ADMA.201906646.

[32] J. Xie, H. Zhang, S. Li, R. Wang, X. Sun, M. Zhou, J. Zhou, X.W. Lou, Y. Xie, Defect-rich MoS_2 ultrathin nanosheets with additional active edge sites for enhanced electrocatalytic hydrogen evolution, Adv. Mater. 25 (2013) 5807–5813, https://doi.org/10.1002/ADMA.201302685.

[33] K. Wu, W. Wang, H. Guo, Y. Yang, Y. Huang, W. Li, C. Li, Engineering Co nanoparticles supported on defect MoS_{2-x} for mild deoxygenation of lignin-derived phenols to arenes, ACS Energy Lett. 5 (2020) 1330–1336, https://doi.org/10.1021/ACSENERGYLETT.0C00411.

[34] W. Zhan, Y. Yuan, B. Yang, F. Jia, S. Song, Construction of MoS_2 nano-heterojunction via ZnS doping for enhancing in-situ photocatalytic reduction of gold thiosulfate complex, Chem. Eng. J. 394 (2020), 124866, https://doi.org/10.1016/j.cej.2020.124866.

[35] W. Zhan, Y. Yuan, X. Yao, B. Yang, F. Jia, C. Lin, J.L. Arauz-Lara, S. Song, Efficient recovery of gold(I) from thiosulfate solutions through photocatalytic reduction with Mn(II)-doped MoS_2, ACS Sustain. Chem. Eng. 9 (2021) 11681–11690, https://doi.org/10.1021/acssuschemeng.1c02160.

[36] F. Zhu, H. Zhang, Z. Lu, D. Kang, L. Han, Controlled defective engineering of MoS_2 nanosheets for rechargeable Mg batteries, J Energy Storage. 42 (2021), 103046, https://doi.org/10.1016/J.EST.2021.103046.

[37] Z. He, R. Zhao, X. Chen, H. Chen, Y. Zhu, H. Su, S. Huang, J. Xue, J. Dai, S. Cheng, M. Liu, X. Wang, Y. Chen, Defect engineering in single-layer MoS_2 using heavy ion irradiation, ACS Appl. Mater. Interfaces 10 (2018) 42524–42533, https://doi.org/10.1021/ACSAMI.8B17145.

[38] L. Li, Z. Qin, L. Ries, S. Hong, T. Michel, J. Yang, C. Salameh, M. Bechelany, P. Miele, D. Kaplan, M. Chhowalla, D. Voiry, Role of sulfur vacancies and undercoordinated Mo regions in MoS_2 nanosheets toward the evolution of hydrogen, ACS Nano 13 (2019) 6824–6834, https://doi.org/10.1021/ACSNANO.9B01583.

[39] S.Y. Cho, S.J. Kim, Y. Lee, J.S. Kim, W. Bin Jung, H.W. Yoo, J. Kim, H.T. Jung, Highly enhanced gas adsorption properties in vertically aligned MoS_2 layers, ACS Nano 9 (2015) 9314–9321, https://doi.org/10.1021/ACSNANO.5B04504.

[40] X. Li, T. Li, Y. Ma, Q. Wei, W. Qiu, H. Guo, X. Shi, P. Zhang, A.M. Asiri, L. Chen, B. Tang, X. Sun, Boosted Electrocatalytic N_2 Reduction to NH_3 by Defect-Rich MoS_2 Nanoflower, Adv. Energy Mater. 8 (2018) 1801357, https://doi.org/10.1002/AENM.201801357.

[41] D. Panchal, A. Sharma, P. Mondal, O. Prakash, S. Pal, Heterolayered TiO_2@layered double hydroxide-MoS_2 nanostructure for simultaneous adsorption-photocatalysis of co-existing water contaminants, Appl. Surf. Sci. 553 (2021), 149577, https://doi.org/10.1016/J.APSUSC.2021.149577.

[42] L. Cai, J. He, Q. Liu, T. Yao, L. Chen, W. Yan, F. Hu, Y. Jiang, Y. Zhao, T. Hu, Z. Sun, S. Wei, Vacancy-induced ferromagnetism of MoS_2 nanosheets, J. Am. Chem. Soc. 137 (2015) 2622–2627, https://doi.org/10.1021/JA5120908.

[43] B. Sun, Z. Liang, Y. Qian, X. Xu, Y. Han, J. Tian, Sulfur vacancy-rich O-doped 1T-MoS_2 nanosheets for exceptional photocatalytic nitrogen fixation over CdS, ACS Appl. Mater. Interfaces 12 (2020) 7257–7269, https://doi.org/10.1021/ACSAMI.9B20767.

[44] N. Luo, C. Chen, D. Yang, W. Hu, F. Dong, S defect-rich ultrathin 2D MoS_2: The role of S point-defects and S stripping-defects in the removal of Cr(VI) via synergistic adsorption and photocatalysis, Appl Catal B 299 (2021), 120664, https://doi.org/10.1016/J.APCATB.2021.120664.

[45] J. Xiong, Y. Liu, D. Wang, S. Liang, W. Wu, L. Wu, An efficient cocatalyst of defect-decorated MoS_2 ultrathin nanoplates for the promotion of photocatalytic hydrogen evolution over CdS nanocrystal, J Mater Chem A Mater. 3 (2015) 12631–12635, https://doi.org/10.1039/C5TA02438B.
[46] Y. Liang, W. Zhan, Y. Yuan, F. Jia, B. Yang, J.L. Arauz-Lara, S. Song, Manganese and oxygen dual-doping MoS_2 boosts reduction and adsorption activity toward efficient recovery of gold(I) from thiosulfate solutions, J. Alloy. Compd. 928 (2022), 167185, https://doi.org/10.1016/j.jallcom.2022.167185.
[47] E. Sharifpour, H.Z. Khafri, M. Ghaedi, A. Asfaram, R. Jannesar, Isotherms and kinetic study of ultrasound-assisted adsorption of malachite green and Pb^{2+} ions from aqueous samples by copper sulfide nanorods loaded on activated carbon: Experimental design optimization, Ultrason. Sonochem. 40 (2017) 373–382, https://doi.org/10.1016/j.ultsonch.2017.07.030.
[48] M. Roosta, M. Ghaedi, A. Daneshfar, R. Sahraei, A. Asghari, Optimization of combined ultrasonic assisted/tin sulfide nanoparticle loaded on activated carbon removal of erythrosine by response surface methodology, J. Ind. Eng. Chem. 21 (2015) 459–469, https://doi.org/10.1016/j.jiec.2014.03.005.
[49] D. Sun, J. Yuan, T. Wang, M. Peng, S. Zhang, S. Rao, F. Liu, G.J. Cheng, Enhanced performance in perovskites films by defect engineering and charge carrier transportation via pulsed laser doping of 2D MoS_2, Sustain. Mater. Technol. 36 (2023), e00622, https://doi.org/10.1016/J.SUSMAT.2023.E00622.
[50] W. Yuan, J. Kuang, M. Yu, Z. Huang, Z. Zou, L. Zhu, Facile preparation of MoS_2@ Kaolin composite by one-step hydrothermal method for efficient removal of Pb(II), J. Hazard. Mater. 405 (2021), 124261, https://doi.org/10.1016/J.JHAZMAT.2020.124261.
[51] E. Sharifpour, H.Z. Khafri, M. Ghaedi, A. Asfaram, R. Jannesar, Isotherms and kinetic study of ultrasound-assisted adsorption of malachite green and Pb^{2+} ions from aqueous samples by copper sulfide nanorods loaded on activated carbon: Experimental design optimization, Ultrason. Sonochem. 40 (2018) 373–382, https://doi.org/10.1016/J.ULTSONCH.2017.07.030.
[52] M.M. Rao, D.K. Ramana, K. Seshaiah, M.C. Wang, S.W.C. Chien, Removal of some metal ions by activated carbon prepared from Phaseolus aureus hulls, J. Hazard. Mater. 166 (2009) 1006–1013, https://doi.org/10.1016/J.JHAZMAT.2008.12.002.
[53] N.N. Nassar, Rapid removal and recovery of Pb(II) from wastewater by magnetic nanoadsorbents, J. Hazard. Mater. 184 (2010) 538–546, https://doi.org/10.1016/J.JHAZMAT.2010.08.069.
[54] S.A. Drweesh, N.A. Fathy, M.A. Wahba, A.A. Hanna, A.I.M. Akarish, E.A. M. Elzahany, I.Y. El-Sherif, K.S. Abou-El-Sherbini, Equilibrium, kinetic and thermodynamic studies of Pb(II) adsorption from aqueous solutions on HCl-treated Egyptian kaolin, J. Environ. Chem. Eng. 4 (2016) 1674–1684, https://doi.org/10.1016/J.JECE.2016.02.005.
[55] M.R. Abukhadra, B.M. Bakry, A. Adlii, S.M. Yakout, M.A. El-Zaidy, Facile conversion of kaolinite into clay nanotubes (KNTs) of enhanced adsorption properties for toxic heavy metals (Zn^{2+}, Cd^{2+}, Pb^{2+}, and Cr^{6+}) from water, J. Hazard. Mater. 374 (2019) 296–308, https://doi.org/10.1016/J.JHAZMAT.2019.04.047.
[56] N. Kumar, E. Fosso-Kankeu, S.S. Ray, Achieving Controllable MoS_2 Nanostructures with Increased Interlayer Spacing for Efficient Removal of Pb(II) from Aquatic Systems, ACS Appl. Mater. Interfaces 11 (2019) 19141–19155, https://doi.org/10.1021/ACSAMI.9B03853.
[57] J. Lu, K. Mishra, T.N. Hunter, F. Yang, Z. Lu, D. Harbottle, Z. Xu, Functionalization of mesoporous carbons derived from pomelo peel as capacitive electrodes for preferential removal/recovery of copper and lead from contaminated water, Chem. Eng. J. 433 (2022), 134508, https://doi.org/10.1016/j.cej.2022.134508.
[58] Q. Yu, H. Liu, G. Lv, X. Liu, L. Wang, L. Liao, Mechanistic insight into lead immobilization on bone-derived carbon/ hydroxyapatite composite at low and high initial lead concentration, Sci. Total Environ. 900 (2023), 165910, https://doi.org/10.1016/j.scitotenv.2023.165910.
[59] C. Yang, M. Xu, Y. Wang, S. Li, X. Lv, H. Wang, Z. Li, Recyclable hydrogel-MOFs composite beads for selective removal of Pb(II) from water, Chem. Eng. Res. Des. 193 (2023) 540–554, https://doi.org/10.1016/J.CHERD.2023.03.052.
[60] L. Zhang, X. He, Q. Zhou, X. Hu, Fabrication of 1T-MoS_2 nanosheets and the high-efficiency removal of toxic metals in aquatic systems: Performance and mechanisms, Chem. Eng. J. 386 (2020), 123996, https://doi.org/10.1016/J.CEJ.2019.123996.
[61] E. Zhang, Y.C. Wu, H. Shao, V. Klimavicius, H. Zhang, P.L. Taberna, J. Grothe, G. Buntkowsky, F. Xu, P. Simon, S. Kaskel, Unraveling the capacitive charge storage mechanism of nitrogen-doped porous carbons by EQCM and ssNMR, J. Am. Chem. Soc. 144 (2022) 14217–14225, https://doi.org/10.1021/JACS.2C04841.
[62] Y. Cheng, S. Yang, E. Tao, L. Liu, D. Wang, J. Qian, 1T/2H mixed phase MoS_2 in-situ grown on the surface of montmorillonite for selectively removing Pb^{2+}, Mater Today Chem. 24 (2022), 100858 https://doi.org/10.1016/J.MTCHEM.2022.100858.